Optogenetic manipulation of nuclear Dorsal reveals temporal requirements and consequences for transcription

Virginia L Pimmett, James Mcgehee, Antonio Trullo, Maria Douaihy, Ovidiu Radulescu, Angelike Stathopoulos, Mounia Lagha

© 2025. Published by The Company of Biologists | Development (2025) 152, dev204706. doi:10.1242/dev.204706

RESEARCH ARTICLE

Optogenetic manipulation of nuclear Dorsal reveals temporal requirements and consequences for transcription

Virginia L. Pimmett[1,*], James McGehee[2,*], Antonio Trullo[1], Maria Douaihy[1,3], Ovidiu Radulescu[3], Angelike Stathopoulos[2,‡] and Mounia Lagha[1,‡]

ABSTRACT

Morphogen gradients convey essential spatial information during tissue patterning. Although the concentration and timing of morphogen exposure are both crucial, how cells interpret these graded inputs remains challenging to address. We employed an optogenetic system to acutely and reversibly modulate the nuclear concentration of the morphogen Dorsal (DL), homolog of NF-κB, which orchestrates dorsoventral patterning in the *Drosophila* embryo. By controlling DL nuclear concentration while simultaneously recording target gene outputs in real time, we identified a critical window for DL action that is required to instruct patterning and characterized the resulting effect on spatiotemporal transcription of target genes in terms of timing, coordination and bursting. We found that a transient decrease in nuclear DL levels at nuclear cycle 13 leads to reduced expression of the mesoderm-associated gene *snail* (*sna*) and partial derepression of the neurogenic ectoderm-associated target *short gastrulation* (*sog*) in ventral regions. Surprisingly, the mispatterning elicited by this transient change in DL was detectable at the level of single-cell transcriptional bursting kinetics, specifically affecting long inter-burst durations. Our approach of using temporally resolved and reversible modulation of a morphogen *in vivo*, combined with mathematical modeling, establishes a framework for understanding the stimulus-response relationships that govern embryonic patterning.

KEY WORDS: Patterning, Transcription, *Drosophila*, Imaging, Morphogen, Embryo

INTRODUCTION

It is appreciated that multiple factors contribute to spatiotemporal dynamics of morphogen responses, including the temporal alterations to the morphogen gradient itself, dynamics relating to signal transduction, as well as downstream interactions between target genes (Kutejova et al., 2009). In particular, the duration of exposure to the morphogen has been highlighted as a crucial determinant of patterning responses, as exemplified by recent studies on Nodal, BMP and Bicoid morphogens (Economou and Hill, 2020; Huang et al., 2017). However, how the morphogen gradients are sensed, both in terms of their local concentration and the critical window they must be interpreted within to drive cell-fate decision making, remains a major question in the field. Furthermore, gene regulatory networks (GRNs) act within responding cells to interpret morphogen signals, and perhaps there is built-in robustness to these systems to accommodate varied morphogen dynamics (Manu et al., 2009). Whether morphogen spatiotemporal dynamics are central to decoding morphogen input into discrete cell fates or, instead, downstream transcriptional responses are the major drivers is a fundamental, yet unresolved, question. Distinguishing between these two alternative and potentially non-exclusive modes of action, involving direct versus indirect morphogen control, requires approaches in which the patterning process can be perturbed and studied in real time.

The dorsoventral axis of the developing *Drosophila* embryo is a well-established example of a morphogen-patterned system in which both the morphogen input and target gene outputs can be followed live in time and space (Fernandez and Lagha, 2019; Schloop et al., 2020; Hoppe et al., 2020). In *Drosophila* syncytial embryos, graded input by Dorsal (DL) is important for activating expression of target genes *snail* (*sna*) and *twist* (*twi*) in ventral regions, *ventral nervous system defective* (*vnd*) in ventrolateral regions and *short gastrulation* (*sog*) in lateral regions (Fig. 1H) (Reeves and Stathopoulos, 2009). In addition to the spatial patterning blueprint encoded by a gradient of nuclear DL levels along the dorsoventral axis, other transcription factors (TFs) also ensure establishment of precise borders and the adoption of distinct cell fates. For instance, in ventral cells, the TFs Twi and Sna instruct the mesodermal fate and the subsequent epithelial-mesenchymal transition program, essential to gastrulation (Leptin and Grunewald, 1990). Moreover, Sna directly represses the transcription of the DL target *sog* in ventral cells, which form the presumptive mesoderm (Bothma et al., 2011; Esposito et al., 2016). This combinatorial action of DL, Sna and other factors such as Zelda increasingly restricts *sog* expression to lateral regions prior to gastrulation (Chopra and Levine, 2009; Yamada et al., 2019).

To orchestrate this complex GRN, the action of DL must be tightly regulated in both space and time. The DL gradient has been shown to be dynamic (Reeves et al., 2012; Kanodia et al., 2009; DeLotto et al., 2007). Although these changes in the gradient over time have been detected, the functional relevance during dorsoventral patterning remains unresolved. Recently, optogenetic tools have been used to manipulate DL levels using an opto-degron (Irizarry et al., 2020; McGehee and Stathopoulos, 2024). However, the irreversible nature of this perturbation inhibits identification of

[1]Institut de Génétique Moléculaire de Montpellier (IGMM), University of Montpellier, CNRS-UMR 5535, 1919 Route de Mende, Montpellier 34293, Cedex 5, France. [2]California Institute of Technology, Division of Biology and Biological Engineering, 1200 East California Boulevard, Pasadena, CA 91125, USA. [3]Laboratory of Pathogens and Host Immunity, University of Montpellier, CNRS, INSERM, 34095 Montpellier, France.
*These authors contributed equally to this work

‡Authors for correspondence (angelike@caltech.edu; mounia.lagha@igmm.cnrs.fr)

V.L.P., 0000-0002-5786-7989; J.M., 0000-0002-9353-1235; A.T., 0000-0001-7560-3859; M.D., 0009-0002-7258-7413; O.R., 0000-0001-6453-5707; A.S., 0000-0001-6597-2036; M.L., 0000-0002-7082-1950

Handling Editor: James Briscoe
Received 4 February 2025; Accepted 12 February 2025

Development (2025) 152, dev204706. doi:10.1242/dev.204706

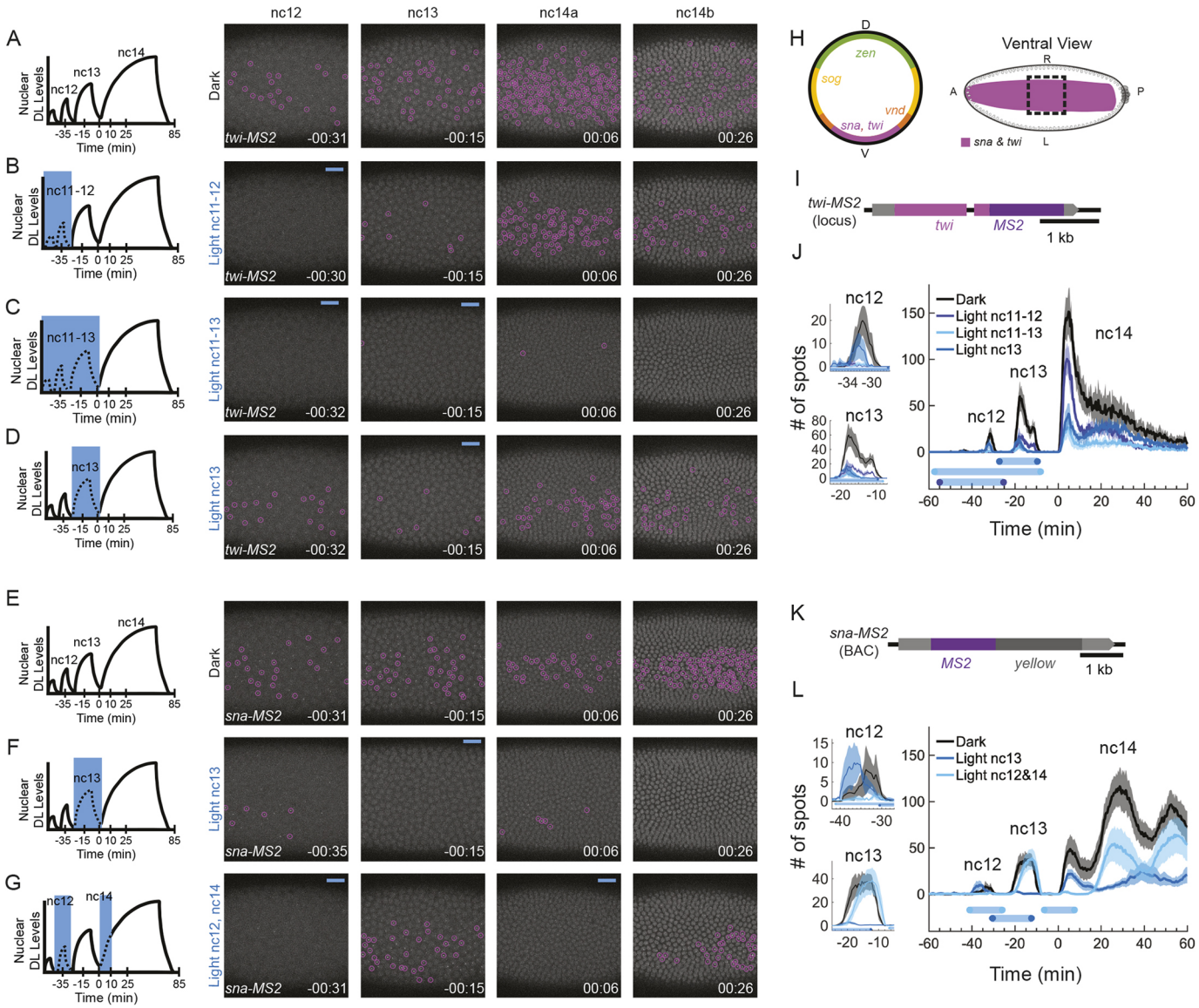

Fig. 1. The critical window for DL activity is nuclear cycle (nc)11-13 for *twi* and nc13 for *sna*. (A-D) *twi-MS2* (magenta) expression in the dark (A), with light at nc11-12 (B), with light at nc11-13 (C) and with light at nc13 (D). (E-G) *sna-MS2* (magenta) expression in the dark (E), with light at nc13 (F), and with light at nc12 and early nc14 (G). (H) Expression domains of DL target genes (left) and the field of view (black dashed line box) used to image *twi-MS2* and *sna-MS2* in the ventral domain (right). A, anterior; D, dorsal; L, left; P, posterior; R, right; V, ventral. (I,K) The *twi-MS2* CRISPR construct (I) and *sna-MS2* large reporter construct (K) used for tracking *twi* and *sna* expression. (J,L) Quantification of the number of active transcription sites (TSs) (mean±s.e.m.) detected for each time frame for *twi-MS2* (J) and *sna-MS2* (L). This metric gives the instantaneous number of active sites of transcription and is not cumulative. The black lines are in the dark (n=3 for *twi*, n=5 for *sna*), the blue lines are with blue light at nc13 (n=3 for *twi*, n=6 for *sna*), the dark-blue line is with blue light at nc11-13 (n=4 for *twi*), and the cyan line is with blue light at nc11-12 (n=3 for *twi*) or nc12 and early nc14 (n=8 for *sna*). The blue bars represent the average illumination window for the matching condition. Nc12 and nc13 are plotted individually on the left as well as with nc14 (right). Nc14 is truncated at 60 min to ensure that no embryo is gastrulating during quantification. Foci are circled in magenta for *sna* and *twi*. t=0 indicates the start of nc14. Illumination schemes are shown to the left of the image stills.

transient critical windows of DL availability (Irizarry et al., 2020). By establishing a reversible optogenetic manipulation paradigm for DL nuclear levels, the current study was able to identify gene-specific temporal requirements for DL across the dorsoventral axis. Timing is a key concept in gene regulation, particularly during development, when the dynamics of morphogens play a pivotal role in shaping gene expression that ultimately leads to patterning. Here, we have identified specific temporal requirements, showing that DL nuclear reduction in nuclear cycle (nc)13 decreases *sna* expression and leads to a change in *sog* stochastic transcription properties in nc14 like decreasing the duration of a long transcriptionally inactive (OFF) state (long inter-burst periods). Our analysis further reveals changes in these transcriptional bursting properties across space, suggesting a mispatterning at the kinetic level. This analysis was only possible through a combination of approaches, including mathematical modeling.

RESULTS

We used DL^{LEXY}, which supports inducible DL nuclear export and is reversible (Fig. S1A-E) (McGehee and Stathopoulos, 2024;

Development (2025) 152, dev204706. doi:10.1242/dev.204706

Niopek et al., 2016; Kögler et al., 2021), together with the MS2/MCP imaging system to monitor spatiotemporal expression of target genes *in vivo* (Lucas et al., 2013; Garcia et al., 2013). In the presence of blue light, DL^{LEXY} is translocated to the cytoplasm, and, when the blue light is removed, $DL^{mCh\text{-}LEXY}$ re-enters the nucleus at levels similar to those before the light was applied (Fig. S2A-D) (McGehee and Stathopoulos, 2024), without significant photobleaching (Fig. S2E). To monitor transcriptional dynamics of DL targets, we focused on four DL targets expressed in ventral, ventrolateral or lateral regions spanning the dorsoventral axis (Fig. 1H). We assayed gene expression of these four targets when blue light was applied during specific embryonic stages to define critical windows of DL action.

The critical window for DL activity is nc11-13 for *twi* and nc13 for *sna*

We first examined the window of time DL must act to support target gene expression in ventral regions of the embryo, within the presumptive mesoderm. We used a published *sna–MS2* large reporter (Bothma et al., 2015) and created a new *twi-MS2* allele by inserting MS2 into the endogenous *twi* locus using CRISPR/Cas9 (Fig. 1I,K; see Materials and Methods). In the dark, *twi-MS2* expression is reliably detected from nc12 through mid-nc14 (i.e. nc14b) but is diminished in nc14 (Fig. 1A, Movie 1). When blue light was applied at nc11-12, *twi-MS2* signal was greatly reduced at nc12 and nc13, but only moderately reduced at nc14 (Fig. 1B). Alternatively, if embryos were exposed to light from nc11 to nc13, *twi-MS2* signal was reduced at nc12, nc13 and nc14, including when returned to the dark during nc14 (Fig. 1C, Movie 1). When illuminated at nc13, *twi-MS2* signal was reduced at nc13 and at nc14, but to a lesser degree than when illuminated from nc11 to nc13 (Fig. 1D,J, Movie 1). This indicated that the DL-critical window for *twi* activation is nc11-13, with nc13 appearing to be more important for the initial peak in *twi* expression than nc11-12. Importantly, the decrease in *twi* transcription under blue light was not due to photobleaching, as demonstrated by our bleaching analysis (Fig. S3A). Taking a similar approach, we found that another ventral target gene, *sna*, exhibited a narrower critical window for DL action. When blue light was shone at nc13, *sna-MS2* signal was greatly reduced at nc13 and nc14 (Fig. 1E-G, Movie 2). Because the number of *sna* transcription sites (TSs) was greatly reduced (Fig. 1L), illuminating embryos from nc11 to nc13 was not necessary. Thus, reduction of DL levels in this short window of ∼15-20 min (nc13) was sufficient to silence *sna* transcription in nc13 and drastically reduce expression at subsequent stages. We also observed that the occurrence of gastrulation was reduced in embryos illuminated at nc13 (Fig. 2A-D). We believe that these gastrulation defects are due to the absence of Sna protein, elicited by DL nuclear reduction in nc13. We confirmed the absence of Sna protein with a more sustained light exposure of DL^{LEXY} embryos with a blue-light box set-up (Fig. S1F; see Materials and Methods). Therefore, although both *twi* and *sna* target genes are expressed in ventral regions in which high levels of nuclear DL are present, these genes exhibit different temporal dependencies, with DL needing to act earlier to support *twi* and only later to support *sna*.

Next, we asked whether the time of DL action or the duration of this input signal is the critical factor driving *sna* expression. To discriminate between these two alternatives, DL was exported with blue light in nc12 as well as in early nc14 within the same embryo, for a total duration of 26.3±1.0 min (mean±s.e.m.), ∼6 min longer than the length of time blue light was given during a complete nc13 cycle duration, which was 20.5±0.6 min (mean ±s.e.m.). When we illuminated embryos with blue light during nc12 and a second time at early nc14, *sna* expression was able to recover during nc13 and late nc14 (Fig. 1G,L, Movie 2). A similar experiment could not be performed for *twi*, as *twi* expression is difficult to detect at mid to late nc14 and recovery of *twi* expression would not be observable after removal of blue light. These results support the hypothesis that the timing of DL input in nc13 is crucial for *sna* expression.

vnd and *sog* persist during nc14 despite reduced nuclear DL levels at nc13

Having defined the critical temporal window required to activate ventral targets, we next questioned whether the action of DL at nc13 was also important for ventrolateral and lateral targets. To this end, we imaged *vnd*, a DL target expressed in the ventrolateral domain, and *sog*, which is expressed in the lateral domain (Fig. 1H). We employed a reporter transgene to follow *vnd* expression in early embryos based on output of a single enhancer (*vndNEE-MS2*) (Falo-Sanjuan and Bray, 2022) (Fig. 2E) and used published fly stocks with MS2 engineered into the *sog* locus (*sog-MS2*) (McGehee and Stathopoulos, 2024; Whitney et al., 2022) (Fig. 2J). Because *vndEEE* is a reporter for which the proximity of the enhancer and promoter is different, the effects of light might not represent the true expression of the endogenous locus.

When assayed using DL^{LEXY} with illumination on the ventral side (Fig. 2F,K), we observed that *vnd* and *sog* responded differently to removal of DL. *vndEEE* expression was acutely decreased in the presence of blue light when it was applied at either nc13 or parts of nc14, but there was no lasting effect as observed for *sna* (Fig. 2G-I, Fig. S4), regardless of whether *vndEEE* was imaged ventrolaterally or ventrally (Fig. 2F, Fig. S4B, Movie 3). We quantified the number of active *vndEEE* nuclei at nc14 and found that it appeared largely unaffected by removal of DL at nc13 (Fig. 2H). A previous study showed that no matter how long the blue light is shone on DL^{LEXY} embryos, *sog* expression is retained (e.g. for the entirety of nc13-14) (McGehee and Stathopoulos, 2024). Even though DL^{LEXY} is predominantly cytoplasmic under blue light, there is some residual, low-concentration DL in the nucleus (McGehee and Stathopoulos, 2024) (Fig. S2). This small amount of transient DL might be sufficient to support *sog* transcriptional activation. When embryos were illuminated with blue light on the ventral side, some *sog* was detected in regions in which it should be repressed (Fig. 2K-N, Movie 3). The number of *sog*-active TSs was higher with light at nc13 compared with the dark condition (Fig. 2M). Because we previously did not observe a change in *sog* expression with removal of DL (McGehee and Stathopoulos, 2024), and the number of *sog* TSs increased instead of decreasing, this suggests a loss of repression under blue light in ventral regions.

These experiments were able to define distinct temporal requirements for DL in supporting the activation of two target genes. DL action is required early at nc11-13 for *twi* and at nc13 for *sna*. If DL levels are reduced during these time windows, then respective gene expression is reduced at nc14 (Fig. 1J,L). In contrast, nc13 was not crucial for activation of the ventrolateral and lateral DL target genes *vnd* and *sog*. For nc13 and nc14, DL input to *vndEEE* is acutely required, but there is no long-term memory effect and reporter expression recovers once DL is available again (Fig. 2H). The number of nuclei exhibiting an active *sog* TS was apparently refractory to a reduction of DL levels, even during blue-light illumination. In fact, reducing DL levels on the ventral side led to an increase in *sog* TSs, likely due to a loss of Sna (Fig. 2M, Fig. S1F-G).

Development (2025) 152, dev204706. doi:10.1242/dev.204706

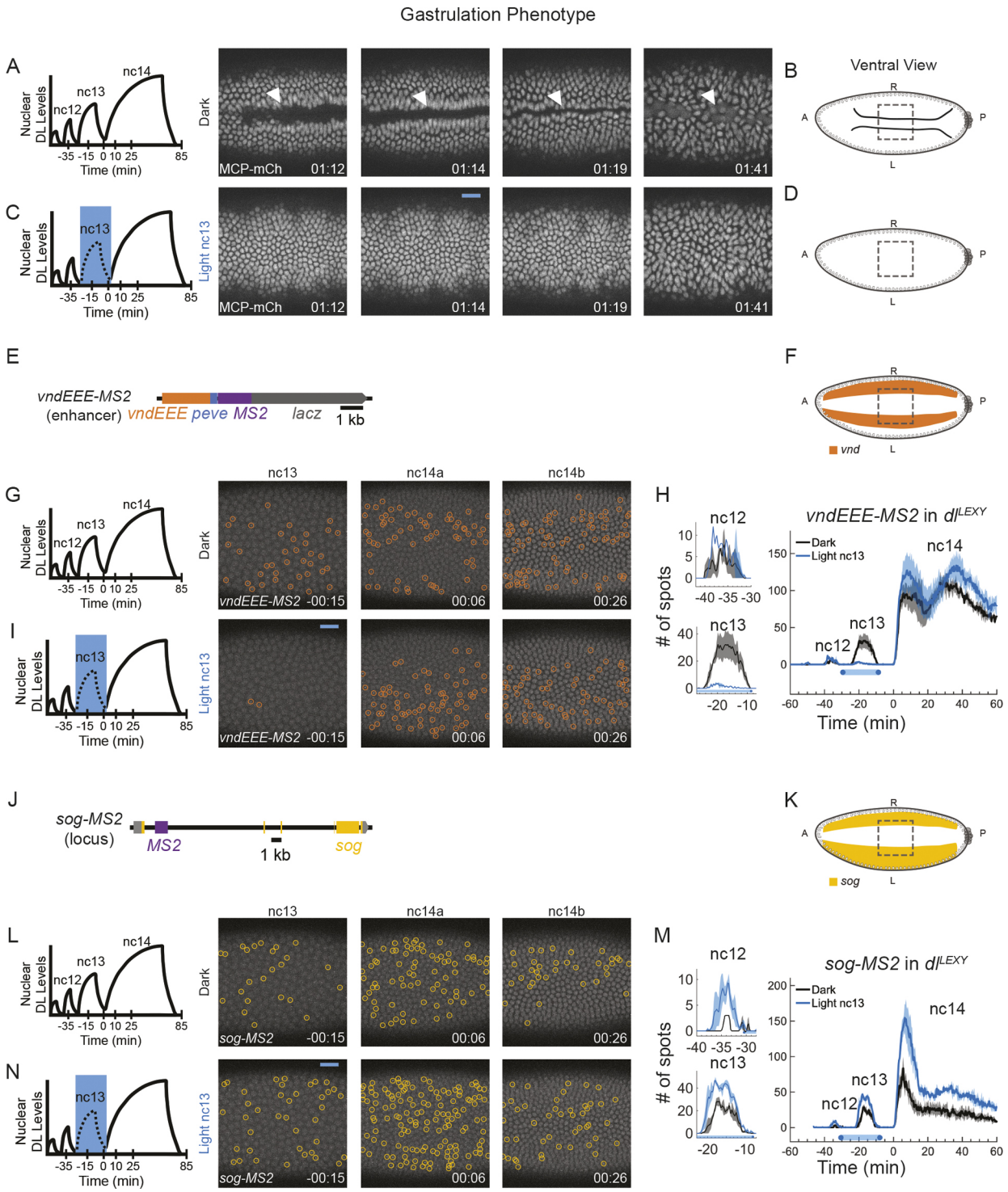

Fig. 2. *vnd* and *sog* are retained at nc14 despite reduced nuclear DL levels at nc13. (A,C) *dl*^{LEXY}*; MCP-mCherry*/*TM3* was imaged for the MCP-mCherry signal with no MS2 crossed in to determine what effect the light had on gastrulation. Embryos in the dark do not have gastrulation defects (A; *n*=0/3 embryos have gastrulation defects), whereas embryos with light shone at nc13 fail to gastrulate completely (C; *n*=3/4 embryos have gastrulation defects). White arrowheads indicate the location of gastrulation. (B,D) Schematic representing gastrulation (B) or a failure to gastrulate (D), and the field of view (dashed line boxes). (E,J) The *vndEEE-MS2* reporter construct (E) and the *sog-MS2* CRISPR construct (J) used for tracking *vnd* and *sog* expression. (F,K) Schematic of the field of view used to image ventrally for *vnd* (F) or *sog* (K). (G,I,L,N) Expression in the dark at nc13 and nc14 for *vndEEE-MS2* (G) and *sog-MS2* (L) or when illuminated with blue light at nc13 for *vndEEE-MS2* (I) and *sog-MS2* (L). Foci are circled in orange for *vnd* and yellow for *sog*. (H,M) Quantification of the number of active TSs detected for *vndEEE-MS2* (H) or *sog-MS2* (M). The black lines are in the dark and the blue lines are with blue light at stages indicated (mean±s.e.m.; *n*=3 embryos for each). Nc12 and nc13 are plotted individually on the left as well as with nc14 (right). Nc14 is truncated at 60 min to ensure that no embryo is gastrulating during quantification. *t*=0 indicates the start of nc14 (A,C,G,I,L,N).

Development (2025) 152, dev204706. doi:10.1242/dev.204706

Reduction of DL levels in nc13 does not affect the kinetics of *sog* transcription at nc13

Although this quantification suggests that the probability of activating the transcription of the *sog* promoter is insensitive to blue light-induced DL nuclear export, it cannot determine whether a more subtle effect operates at the level of transcriptional kinetics. For instance, it is well appreciated that most genes are transcribed in a discontinuous manner with bursts occurring at various timescales (Meeussen and Lenstra, 2024). Like other developmental genes, endogenous *sog* also exhibits a bursty transcription in the early embryo (Fig. 3F,H, Movie 4) (Whitney et al., 2022; Forbes Beadle et al., 2023). Analysis of live transcription signals shows that transcription activity is intermittent, alternating between active and several inactive periods. Mathematical models can capture this process, termed 'bursting', and characterize both the probability and durations of the active and inactive transcriptional periods. In addition, as *sog* was the only target gene that remained on during blue light, it was the best candidate for this analysis. Therefore, we further investigated the bursting behavior of *sog* when nuclear DL^{LEXY} levels were perturbed by blue light at nc13, with the understanding that this would lead to a substantial reduction in *sna* expression but only a partial reduction in *twi*. To examine *sog* bursting kinetics, we imaged its transcription with high temporal resolution. Such a fast imaging set-up inevitably leads to bleaching when using a red fluorescent detector, such as the MCP-RFPT employed here. However, our bleaching study demonstrated that, prior to 20 min into nc14, less than 20% of bleaching is observed, allowing adequate detection (Fig. S3B).

Because *sog* is expressed in nc13 throughout ventral and lateral regions (the presumptive mesoderm and neurogenic ectoderm) with

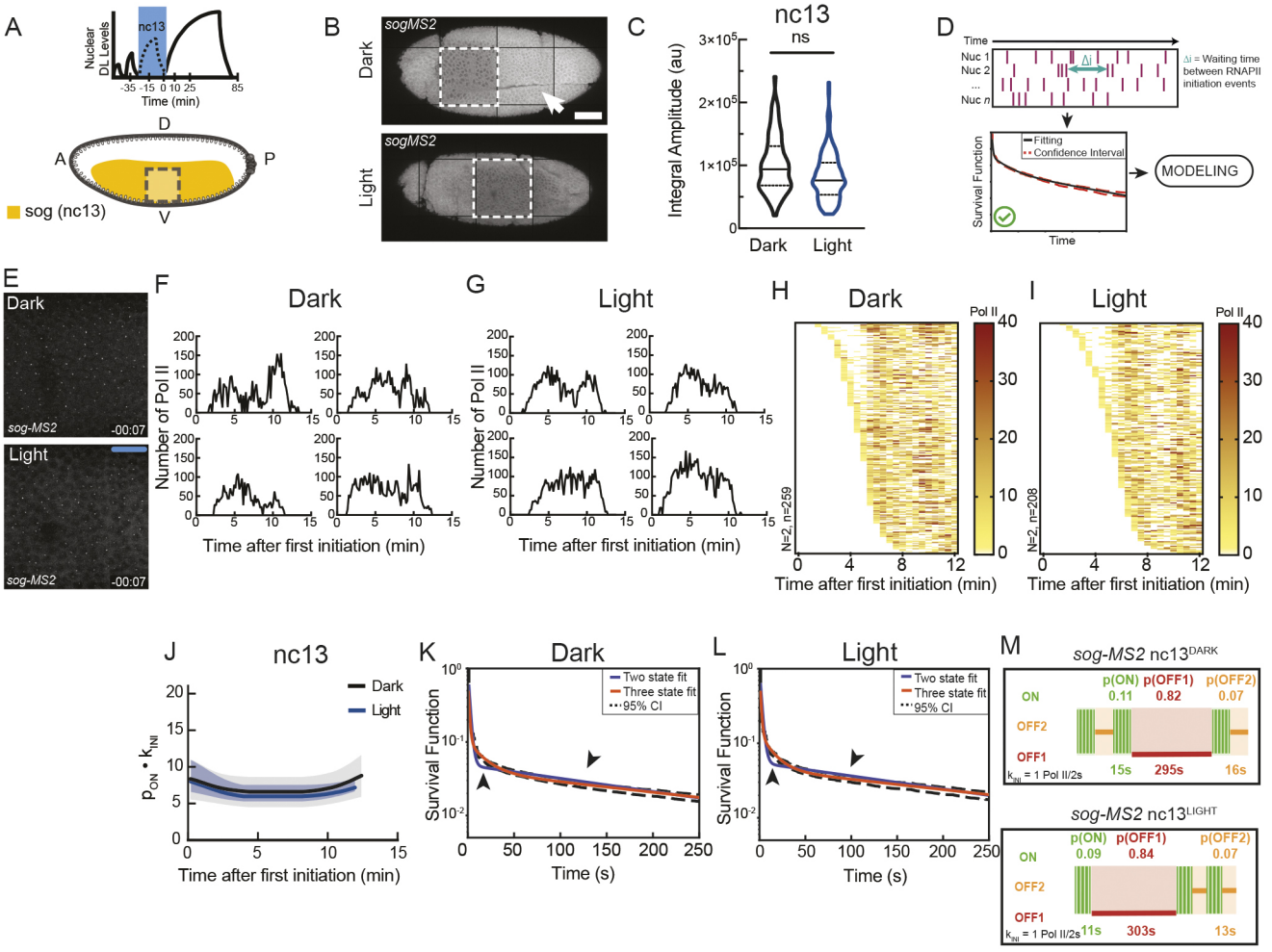

Fig. 3. Reduction of DL levels in nc13 does not acutely perturb *sog* bursting kinetics at nc13. (A) Schematic of blue-light (DI export) window during nc13. (B) Tilescan of late nc14 embryos showing gastrulation in control (top) and attempted gastrulation (bottom) after DL export in nc13. Arrowhead indicates invagination associated with gastrulation that is absent following DL export. Dashed boxes indicate imaging region. Scale bar: 50 µm. (C) Integral amplitude of *sog-MS2* transcription in nc13 (ns, not significant; Kolmogorov–Smirnov test). au, arbitrary units. (D) Schema showing the process of model fitting from statistical deconvolution of individual nuclei traces. (E) *sog-MS2* transcription in control (top) or DL-exported (bottom) conditions during nc13. (F,G) Sample single nuclei *sog* transcriptional traces in nc13 for control (F) and DL-exported (G) conditions. (H,I) Heatmaps showing the number of polymerase initiation events for *sog* in nc13 in control (H) and DL-exported (I) conditions. Each row represents one nucleus, and the number of RNA polymerase II (Pol II) initiation events per 30 s bin is indicated by bin color. (J) Kinetic parameter stability as a function of time for *sog-MS2* transcription expressed as the product of the probability to be active (p_{ON}) and the Pol II initiation rate (k_{INI}) in nc13 in control (black) or DL-exported (blue) conditions. (K,L) Survival function for the distribution of waiting times between polymerase initiation events for *sog-MS2* transcription in control (K) or DL-exported (L) conditions. Two-exponential fitting (blue) estimated using the Kaplan–Meier method extends beyond (arrowheads) the 95% confidence interval (CI; dashed lines) and is rejected. (M) Ideograms of nc13 *sog-MS2* transcriptional kinetics in dark (control; top) or light (DL-exported; bottom) conditions. Live imaging: dark, *N*=2 embryos, *n*=259 nuclei; light, *N*=2 embryos, *n*=208 nuclei.

Development (2025) 152, dev204706. doi:10.1242/dev.204706

no respect to the future differentiation of these two presumptive domains, we pooled *sog*$^{+}$ nuclei (with an active TS) for kinetic profiling from the entire imaging window spanning ventral to ventrolateral regions (Fig. 3A,B, dashed line boxes). Owing to the absence of fluorescently labeled nuclear markers, we were unable to orient live transcription traces relative to mitosis and thus traces were tracked relative to the first detected transcriptional activation event in each nuclear cycle.

As discussed above, the number of active nuclei expressing *sog* increased in nc13 when nuclear DL levels were perturbed with blue light (Fig. 2M). We also quantified the integral amplitude in nc13 for each trace, which is a proxy for total mRNA output, and noted no difference in total *sog* mRNA output (Fig. 3C). This was confirmed by quantifying nascent *sog* transcription using single-molecule fluorescence *in situ* hybridization (smFISH) (Fig. S5), where extended (2 h) DL export did not result in substantial perturbations to *sog* nascent transcription compared with the control. Thus, the embryo-level transcription of *sog* appears to be unaffected by optogenetic removal of DL.

However, *sog* transcription is bursty, meaning that the fluctuations, not just the mean mRNA production, could be biologically relevant. Therefore, we next turned to a previously established mathematical modeling approach to examine the underlying kinetic parameters of *sog* transcriptional bursting at the single-nucleus level when the DL gradient was perturbed. During a given nuclear cycle, the MS2 signal that carries information on the bursting kinetics progresses through several stages. Initially, following mitotic exit, no signal is detected and this period corresponds to time for DNA replication and resumption of transcription. This period is typically modeled by considering the distribution of the time to reactivation (Dufourt et al., 2021). Following this initial period, transcription builds up at each transcription foci until reaching a stationary phase, during which the signal remains stable. Bursting during this stationary phase is analyzed using BurstDECONV (Douaihy et al., 2023).

We used BurstDECONV (Douaihy et al., 2023) to deconvolve *sog-MS2* signal, i.e. reconstruct the sequential polymerase initiation events contributing to this signal (Fig. 3D) (Douaihy et al., 2023). The deconvolution relies on a model of the contribution of a single polymerase to the MS2 signal, which depends, among other factors, on the length of the transcribed MS2 and post-MS2 sequences. Because the MS2 loops were inserted in the first intron of *sog*, an additional point of consideration for the modeling was to understand the gene's splicing, recently observed to be largely recursive in human cells (Wan et al., 2021). We ensured that *sog* splicing was not recursive at this stage by consulting native elongating transcript sequencing technology (NET-seq) data from *Drosophila* embryos (Prudêncio et al., 2022). Instead, *sog* splicing likely occurs at intron-exon junctions and is co-transcriptional, as supported by fluorescence *in situ* hybridization (FISH) data (Bothma et al., 2011).

Furthermore, the deconvolution method implemented by BurstDECONV assumes that the signal is stationary. Therefore, we first determined whether *sog* transcription in nc13 (Fig. 3E-I) reached stationary dynamics by plotting the mean waiting time between polymerase initiation events for a short window (82 s; Fig. 3J). This represents the mean transcription rate for each window, expressed as the product of the RNA polymerase II (Pol II) initiation rate (k_{INI}) in the active state and the probability of a nucleus to be active (p_{ON}). Transcription is considered stationary if this value remains stable across sequential time windows. Indeed, this demonstrated that in both dark (nuclear DL; Fig. 3J, black) and light (DL-exported; Fig. 3J, blue) conditions, the underlying kinetic dynamics reached stationarity.

Having established the specific window exhibiting stationarity of the *sog* signal, we next sought to extract *sog* promoter switching rates. To access *sog* transcription kinetics, we examined the distribution of waiting times between Pol II initiation events during the first 15 min of nc13 and fitted it with a multi-exponential function (Fig. 3K,L). The multi-exponential fitting gives access to the kinetic parameters driving *sog* transcription, such as the duration of the productive (ON) and non-productive (OFF) states, as well as the Pol II firing rate in the ON state. Crucially, this approach does not presume a specific number of states *a priori*, but instead discovers it as an emergent property of the data themselves, resulting from the number of exponentials needed to fit the data. In both dark (nuclear DL) and light (DL export), this distribution could not be fitted by a bi-exponential distribution, indicating that the classical two-state random telegraph promoter model is insufficient to fit the data. A three-exponential fitting, corresponding to a three-state model, was sufficient, however, for both the nuclear and exported DL cases (Fig. 3K,L, compare blue and orange curves). This three-state promoter scheme consists of a competent ON state and two distinct OFF states, each characterized by a different mean duration: OFF1 (long-lived, 295-303 s) and OFF2 (short-lived, 13-16 s). In terms of probability, the prolonged inactive state (OFF1) is the most probable state, dominant in both dark and light conditions (Fig. S6J-L). When nuclear DL levels were reduced with blue light in nc13, *sog* promoter bursting dynamics were also captured by a three-state model with similar kinetics to those observed in the dark (Fig. 3M). This analysis of *sog* transcriptional dynamics suggests that upon optogenetic perturbation of DL with the LEXY system in nc13, *sog* transcriptional kinetics are not acutely affected.

DL export in nc13 leads to mispatterning in nc14, accompanied by a change in bursting kinetics

While in nc13, *sog* is expressed throughout the presumptive mesoderm and neurogenic ectoderm; it is progressively repressed in the nc14 mesoderm via increasing levels of Sna but maintained in the neurogenic ectoderm (McHale et al., 2011). Given the specific requirement of DL in nc13 to promote the expression of *sna*, and by extension the repression of *sog* in nc14, we examined the transcription of *sog* in nc14 when nuclear DL levels are perturbed in nc13 (Fig. 4A).

Because *sog* is known to have variable expression dynamics based on the tissue in which it is expressed (Whitney et al., 2022; McHale et al., 2011; Dunipace et al., 2019), we began by examining *sog* repression exclusively in the presumptive mesoderm. In dark embryos, we identified the mesoderm/neuroectoderm boundary based on repression of *sog* by Sna in the mesoderm and spatially selected only those nuclei located in the presumptive mesoderm (see Fig. 4B). In illuminated embryos, the mesoderm/neuroectoderm boundary driven by Sna protein is perturbed due, at least in part, to changes in *sna* expression and thus cannot be used to differentiate the tissues. To circumvent this, embryos were imaged with the presumptive ventral furrow oriented to one edge of the imaging window, and the mesoderm was selected as the 30 µm to either side of the failed furrow at the end of nc14. As expected, given the reduction in *sna* transcription, we observed extended maintenance of *sog* transcription in the presumptive mesoderm under illumination compared with the control dark condition (Fig. 4C). *sog* derepression in the ventral part of the embryos was also observed by an alternative approach not relying on MS2/MCP imaging. We performed smFISH in DL^{LEXY} embryos with a more sustained light exposure using an optobox (Fig. S5A-C). Interestingly, in these conditions, the quantification of TS intensities suggests that, in the light, transcription of *sog* in ventral nuclei is not

Development (2025) 152, dev204706. doi:10.1242/dev.204706

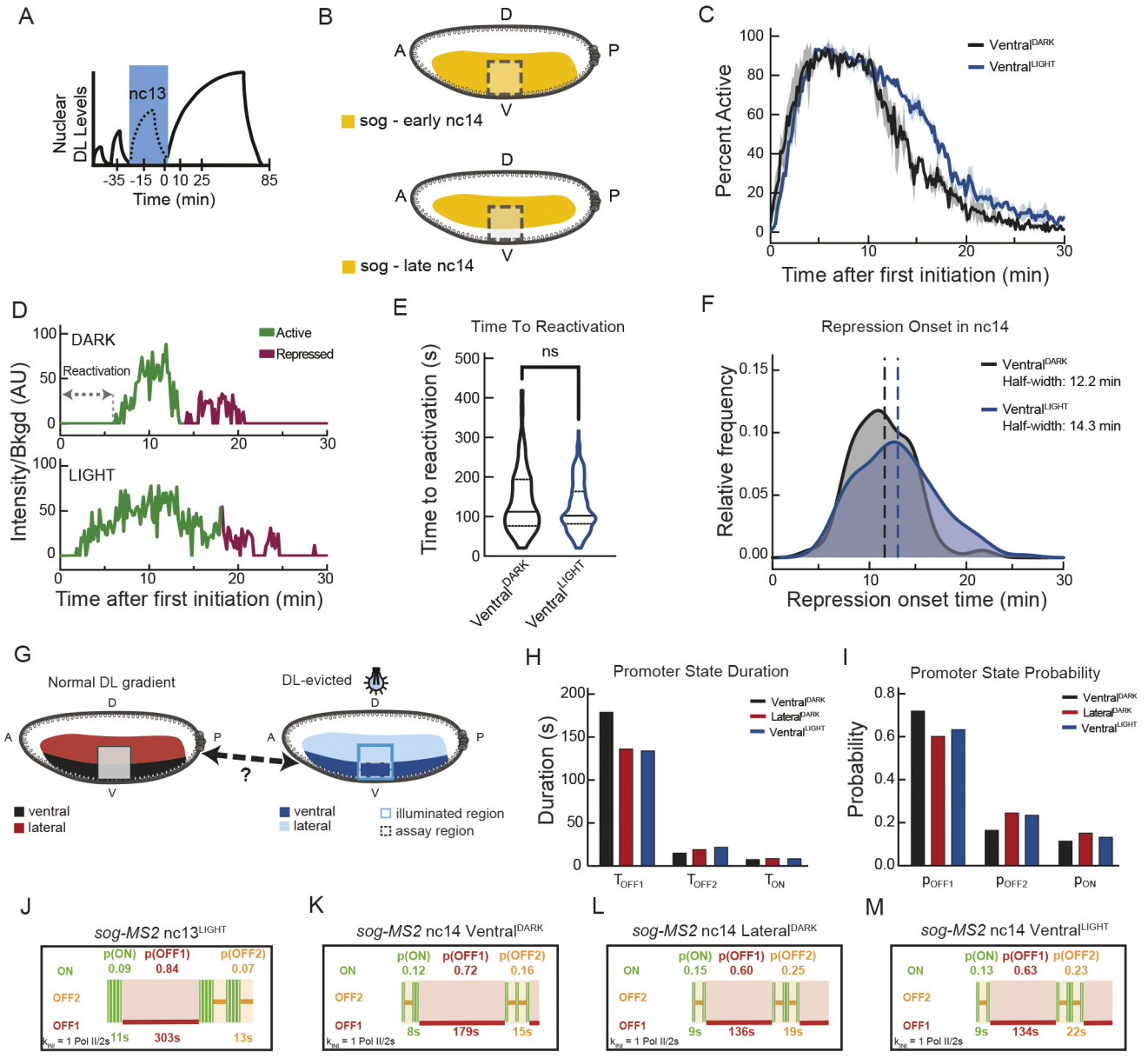

Fig. 4. Dorsal export in nc13 is sufficient to transform *sog* kinetics in the mesoderm in nc14. (A,B) Schematic of blue light (A; DL export) and analysis window (B; dashed line boxes) for the same movies used in Fig. 3 but during nc14 within the indicated embryonic region. (C) Fraction of active nuclei in ventral domain in control (black) or DL-exported (blue) conditions, shown as mean±s.e.m. Representative insets show relative intensity of *sog* transcription in control (black) or DL-exported (blue) conditions at indicated times. (D) Single-nuclei traces indicating the time to reactivation and breakpoint between active and repressed paradigms. (E) Distribution of time to reactivation for control and DL-exported ventral nuclei (ns, not significant; Kolmogorov–Smirnov test). (F) Distribution of breakpoint times for initiation of stable repression in nc14 in control (black) and DL-exported (blue) conditions using Bayesian change point detection. Dashed lines indicate median breakpoint times. (G) Schema indicating potential equivalency between Lateral^{DARK} and Ventral^{LIGHT} domains. (H) Promoter state durations for Ventral^{DARK}, Ventral^{LIGHT} and Lateral^{DARK} domains for the first 15 min of active *sog* transcription in nc14. (I) Promoter state probabilities for Ventral^{DARK}, Ventral^{LIGHT} and Lateral^{DARK} domains for the first 15 min of active *sog* transcription in nc14. (J-M) Ideograms of nc13^{LIGHT} (J) and nc14 *sog-MS2* transcriptional kinetics in dark (K,L; control) or light (M; DL-exported) conditions. Live imaging: dark, *N*=2 embryos, *n*=70 nuclei for ventral domain; light, *N*=2 embryos, *n*=162 nuclei for ventral domain, *n*=181 nuclei for lateral domain.

different from that in more laterally located nuclei in the dark (Fig. S5E-G).

To understand how reducing DL levels in nc13, and the subsequent reduction of nc14 Sna protein levels (Fig. S1F,G), affects *sog* transcription dynamics in nc14, we characterized two metrics from the movies for each nucleus: the time to reactivation (Fig. 4D, double-arrow domain) and the repression breakpoint (Fig. 4D, switch from green to red trace), corresponding to the post-mitotic transcription reactivation and to the onset of repression, respectively. We first considered the timing required to reach the first transcriptional activation after mitosis, which we call the time to reactivation (Dufourt et al., 2018) (Fig. 4E). This time was not significantly different between the control (dark) and DL-exported (light) nuclei. This reactivation time has two components: a deterministic component common to all nuclei and a stochastic component (Dufourt et al., 2018). Although both components contribute to the reactivation period duration, only the stochastic component depends on the number and duration of rate-limiting

Development (2025) 152, dev204706. doi:10.1242/dev.204706

steps in reassembling the transcriptional machinery (Bellec et al., 2018; Lammers et al., 2020). The reactivation metric used here accounts only for the stochastic part of *sog* expression in early nc14 when nuclei reinitiate *sog* expression following mitosis. Indeed, time zero is defined here as the moment when the first nucleus resumes transcription after mitosis. By making this choice, we exclude the deterministic component of the reactivation time, which is consistent across all nuclei.

We then turned to Bayesian change point detection (BCPD) to determine the onset of repression, when each individual nucleus underwent a transition from building up repression to stable, full repression (Pimmett et al., 2024 preprint; Adams and MacKay, 2007 preprint). For further modeling purposes, the signal is considered stationary after the repression onset. In the DL-exported (light) nuclei, we observed that repression onset for *sog* was significantly delayed (Fig. 4F, dashed lines). Moreover, upon DL export in 13, *sog* repression within the ventral region appeared much less coordinated (i.e. the repression onset showed greater internuclear variability) in nc14 than in dark conditions (Fig. 4F). Thus, acute reduction of DL levels in the short temporal window spanning nc13 has a substantial, persistent impact on the dynamics of *sog* transcription later in nc14.

Because DL export in nc13 affects *sna* expression (Fig. 1F, Fig. S1F,G) and because Sna and Twi are important drivers of the mesodermal fate (Kosman et al., 1991; Rembold et al., 2014), we expect that the DL-depleted ventral cells could have either 'lost' or failed to acquire a mesodermal fate and instead adopted a more lateral-like fate (Fig. 4G). To test this hypothesis at the kinetic level, we sought to extract the transcriptional bursting kinetics for *sog* in various spatial regions of the embryo at stationarity in nc14 when kept in the dark or exposed to light at nc13. Ventral region nc14 *sog* data in embryos previously exposed to light in nc13 ($Ventral^{LIGHT}$) or continuously kept in the dark ($Ventral^{DARK}$) were compared with those from lateral regions (i.e. $Lateral^{LIGHT}$ and $Lateral^{DARK}$). Because embryos failed to gastrulate when exposed to light (i.e. there was limited ventral furrowing), the lateral region was confidently identifiable only in embryos kept in the dark ($Lateral^{DARK}$).

We used BurstDECONV (Douaihy et al., 2023) to convert individual fluorescent traces into polymerase initiation events (Fig. S6A-F) from which kinetic parameters can be modeled (Douaihy et al., 2023) for the three conditions: $Ventral^{DARK}$, $Ventral^{LIGHT}$ and $Lateral^{DARK}$ at stationarity in nc14 (see Materials and Methods; Fig. 3D, Fig. S6D-F). After model fitting (Fig. S6J-L), both the control and DL-exported nuclei required a three-state fitting with a competent ON state as well as both long (minutes) and short (seconds) OFF states. In the dark, the *sog* promoter seemed to transition between three promoter states in both nc13 and nc14; however, the duration and probabilities of the dominant long OFF state were different between these two cycles (Fig. 4H-M, Fig. S6M-O). After DL export in nc13, we observed that the duration of the long non-productive (OFF1) state in nc14 was reduced by 25%, and its probability was decreased by 12% in the ventral domain. Furthermore, the duration of the short non-productive (OFF2) state in nc14 was slightly increased, and its probability was significantly increased by 42% in the ventral domain (Fig. 4H,I, compare $Ventral^{DARK}$ with $Ventral^{LIGHT}$). Notably, these trends associated with the ventral domain after light exposure closely matched the dynamics of the lateral domain control (Fig. 4H,I, compare $Ventral^{LIGHT}$ with $Lateral^{DARK}$). Collectively, these results suggest that *sog* transcription in the ventral region converts to a more lateral-like transcriptional profile in nc14 following transient depletion of DL in nc13.

DISCUSSION

Using an optogenetic approach to control DL localization with LEXY *in vivo* (Fig. 5A), we identified specific time windows in which DL input is essential for the expression of select DL targets expressed in ventral regions (*sna* and *twi*; Fig. 1, Fig. 5B). In contrast, we found that lateral genes like *vnd* and *sog* do not respond in the same way as ventral genes to the narrowest critical window of DL activity (i.e. nc13) (Fig. 2, Fig. 5B). Additionally, we characterized the spatiotemporal bursting kinetics of the endogenous gene *sog* gene across different stages of the patterning process (Fig. 5C). Notably, when DL is displaced from the nucleus early on, *sog* is derepressed in ventral regions at later stages, resulting in mispatterning. This mispatterning causes ventral cells, the presumptive mesoderm, to instead exhibit properties characteristic of neurogenic ectoderm. These shifts in identity were quantifiable by changes in bursting kinetic properties, with ventral cells adopting a kinetic profile usually associated with lateral cells. These findings were supported by the observation that light exposure at nc13 leads to gastrulation defects, likely because ventral cells can no longer undergo the cell shape changes necessary to support invagination (Fig. 2A,C).

These results echo, but are distinct from, the temporal requirement identified for the Bicoid morphogen that controls patterning along the anterior-posterior axis of *Drosophila* embryos. Duration of Bicoid input is important for targets expressed at the anterior pole, presumed to be high threshold targets (Huang et al., 2017). However, we found that *sna*, a presumed high-threshold DL target gene, is not sensitive to duration of DL input before mid nc14, as ∼25-30 min blue light exposure during nc12+nc14 early did not turn off *sna*, whereas a less than 20 min exposure during nc13 did. Instead, our data support the view that *sna* and *twi*, both expressed in ventral regions, require DL input at a critical time (i.e. nc13 for *sna* and nc11-13 for *twi*) when DL activity is necessary so that *sna* and *twi* can be expressed later at nc14. It is notable that *sna* and *twi* exhibit different critical windows of DL input despite being both high-threshold DL targets. We propose that this relates to combinatorial control by other TFs in addition to DL, including opposite autoregulatory activities. *twi* is known to exhibit positive autoregulatory feedback, whereas *sna* is known to exhibit negative autoregulatory feedback (Leptin, 1991). We suggest that if a little Twi or Sna is made at or following the time that DL is removed at nc13, the respective autoregulatory feedbacks might lead to retention of *twi* and loss of *sna* transcripts. Therefore, the simplistic model of threshold responses to DL is not sufficient to predict whether or not a gene will be retained when DL is perturbed. Previously, we showed that *sna* also exhibits DL dependence at early nc14 using an optogenetic approach based on degradation (Irizarry et al., 2020). Therefore, although DL activity at nc13 is required, it is likely not sufficient for correctly activating *sna*.

There are a number of possible explanations for why DL is crucial at nc13. One is that DL supports an epigenetic change or performs some other pioneering activity at the *sna* locus only possible at nc13 that is required for later expression of *sna* at nc14. Although it remains unclear why the DL level of mother nuclei at nc13 has an effect in nc14, we can envisage several potential molecular mechanisms including mitotic bookmarking (e.g. GAF) (Bellec et al., 2022), mitotic-assisted repression (Esposito et al., 2016), 'memory' transcription hubs (Javier deHaro-Arbona, 2024), or post-transcriptional modulation of mRNA or protein half-life. Our results regarding the criticality of nc13 also agree with a previous study that used an optogenetic approach to activate extracellular signal-regulated kinase (ERK) (McFann et al., 2021). Specifically,

Development (2025) 152, dev204706. doi:10.1242/dev.204706

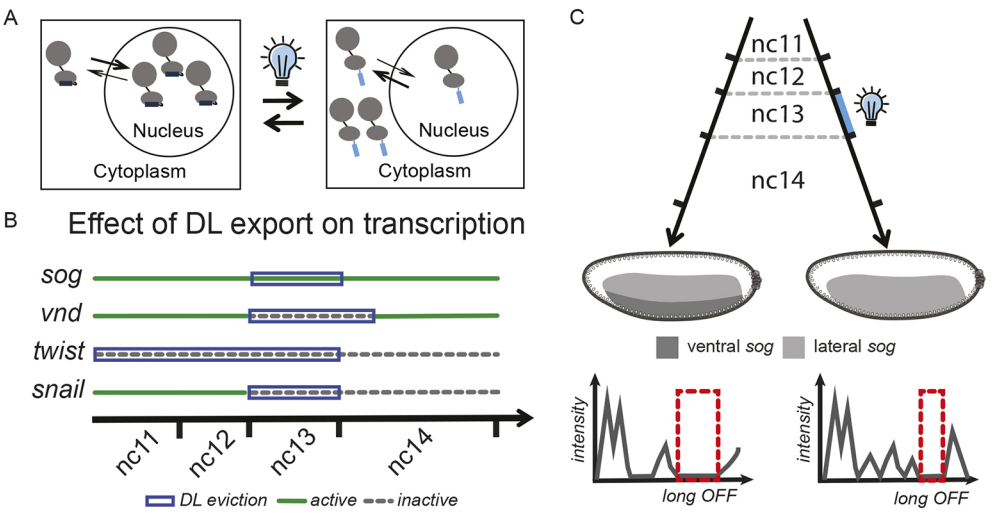

Fig. 5. Dorsal export has differential effects on target gene transcription in early embryogenesis. (A) Schematic of DL^{LEXY} export dynamics upon blue-light stimulation. (B) Summary of pattern-level effects of DL export on transcription of known DL target genes when DL is evicted during critical windows (blue boxes), showing that transcription can remain active (green) or be inactive (dashed gray line). (C) Summary of single cell-level kinetic switching in ventral *sog* transcription in nc14 after blue light is applied in nc13 (right), demonstrating a change of regime from a mesoderm-like to a lateral-like dynamic (i.e. the long OFF1 state is shorter following light treatment).

they found that when light was applied in the trunk at nc13, ectopic expression of *hückebein* (*hkb*), a repressor of *sna*, leads to reduction in *sna* transcription and defects in gastrulation (McFann et al., 2021).

Our inducible and reversible manipulation of a morphogen TF while recording target gene responses allowed us to dissect time-dependent transcriptional dependencies within a complex GRN. Indeed, target gene sensitivity to a dedicated temporal window could be a direct effect or the result of complex feed-forward/combinatorial regulation of other genes by the morphogen input, a common feature of GRNs (Briscoe and Small, 2015; Davidson, 2010). Gene-gene interactions can influence both the timing and duration of critical temporal windows. Using DL^{LEXY} to decrease DL levels and via our characterizations of critical temporal windows, we can study how the GRN responds to reducing the levels of a specific, lineage-driving TF in a system in which DL levels have recovered to their previous level. For instance, *sna* is a crucial component of the GRN acting to support mesoderm formation and a regulator of neurogenic ectoderm and mesectoderm patterning. Sna protein is known to act as a transcriptional repressor, and, without *sna* transcription at nc13 (owing to DL export in nc13), Sna protein levels are diminished in nc14, leading to patterning failure. In this manner, we could distinguish both direct, fast effects of DL perturbation (i.e. reduced expression of targets such as *sna*, *twi* and *vnd*) as well as phenotypes that present later, after blue light is removed and DL nuclear levels are recovered (i.e. ventral expansion of *vnd* and *sog*).

This study also highlights the value of combining transient perturbations with quantitative approaches to explore more subtle effects on single-cell state changes. We used this insight of the critical time window for *sna* in nc13 to study the transcriptional dynamics of other target genes. Hence, we could decode how DL levels affect bursting across time (nc13 versus nc14) but also across space (ventral versus lateral). Indeed, by nc14, *sog* is repressed in the mesoderm (by Sna and potentially other repressors) but kept active in lateral regions, thus offering the possibility to compare bursting kinetics in various spatial domains. In both nc13 and nc14 and regardless of DL levels, *sog* promoter dynamics can be recapitulated by a three-state model, comprising a competent ON state, a short-lived OFF state (seconds) and a longer-lived (minutes) highly probable second inactive state (e.g. Fig. 3K,L, orange lines, Fig. S6J-L). Although our data are unable to demonstrate the biochemical nature of these promoter states, their timescale and sensitivity to DL levels and spatial region provide clues to discuss what they could represent. The competent ON state, from which polymerase initiates, is generally interpreted as the preinitiation complex (PIC)-assembled promoter state. Importantly, whereas other studies propose that the probability to be ON stands as the main parameter underlying transcriptional dynamics (Hoppe et al., 2020; Berrocal et al., 2024; Chen et al., 2023 preprint), our study uncovered changes in the duration of an inactive state.

The only promoter state that shows a clear change following transient DL manipulation is the longer lived OFF1 state. There are several possible interpretations of this result. In the blastoderm, *sog* expression is orchestrated by two enhancers, an intronic and a distal enhancer, both regulated by DL. Interestingly, deletion studies have suggested that, instead of being redundant, these two enhancers integrate activation and repression signals differently (Whitney et al., 2022; Dunipace et al., 2019). For example, the intronic enhancer appears to be the principal enhancer in ventral and ventrolateral regions at nc13. Because the long OFF state changes between nc13 and nc14 (see Fig. 4K-M), we speculate that this state corresponds to enhancer-promoter interactions: a long OFF state in nc13 when expression primarily relies on one enhancer, which could be reduced in nc14 thanks to the combinatorial action of two enhancers modulated by the presence or absence of a repressor (Whitney et al., 2022). The kinetics of these long inactive states (minute range) can possibly provide a clue on the timescale and probabilities of enhancer-promoter encounters (Chopra et al., 2012). An alternative, possibly simpler, explanation interprets the long OFF1 state as DNA-bound repressor molecules. The lifetime of this state in the case of multiple binding sites, representing the time required to clear all the sites, could depend on the number of occupied sites. The concentration of the repressor(s) is thus reflected in this duration, as higher concentrations lead to a longer lifetime.

Limitations to the study

To begin, some features of the DL^{LEXY} construct limit some of the conclusions that can be drawn. Because of the intrinsic nuclear import and export sequences of DL, a fraction of the total DL^{LEXY} protein is always rapidly re-imported to the nucleus after eviction, even under blue-light exposure (McGehee and Stathopoulos, 2024). As a result, the DL^{LEXY} tool cannot achieve a full nuclear depletion of DL levels with light but does support a significant reduction, sufficient to prevent high-threshold DL targets such as *sna* and *twi* from being transcribed normally, but

Development (2025) 152, dev204706. doi:10.1242/dev.204706

perhaps not low enough to challenge low-threshold target *sog*. Additionally, current mathematical modeling approaches employed to decipher promoter switching rates from live-imaging data require a steady-state regime. We therefore had to restrict our analysis of *sog* bursting to a specific temporal window in early nc14, during which *sog* kinetics can be considered stationary. Finally, we want to emphasize that bursting analysis only reveals rate-limiting steps of transcription and does not provide their biochemical nature. Using spatiotemporal comparisons and genetic perturbations, we hypothesize as to what these rate-limiting steps could represent, but this remains to be fully demonstrated.

Taken together, our results demonstrate that optogenetic perturbations with high-resolution imaging and quantitative modeling can dissect how a TF affects target gene transcription dynamics in space and time. When employed in the context of a pivotal morphogen TF, patterning can be disrupted and lead to mispatterning: here, presumptive mesoderm (ventral) to neurogenic ectoderm (lateral), detectable at the level of the kinetics of transcriptional bursting.

MATERIALS AND METHODS

Drosophila stocks

For determining the critical window of DL action, crosses were kept at 18°C. *dl^{LEXY}; nos>MCP-mCherry-nls/TM3* virgins were crossed to *twi-MS2*, *sna-MS2*, *vndEEE-MS2/CyO* or *sog-MS2/y* males (see Table S1). MS2 was added to the endogenous locus to generate *twi-MS2* (this study) and *sog-MS2* (McGehee and Stathopoulos, 2024) using CRISPR/Cas9 (Gratz et al., 2014). *sna-MS2* is a large (~25 kb) reporter construct, which was inserted on the third chromosome, and contains the known regulatory sequences of *sna*, MS2 at the 5′ untranslated region (UTR), and part of the yellow gene (Bothma et al., 2015; Perry et al., 2010). *vndEEE-MS2* is a reporter line containing the *vndEEE* enhancer, the *eve* promoter, MS2 at the 5′ UTR and lacZ (Falo-Sanjuan and Bray, 2022). *dl$^{mch\text{-}LEXY}$* mothers were used to image DL$^{mCh\text{-}LEXY}$ levels.

In all other cases, stocks and crosses were maintained at 25°C. *dl^{LEXY}; nos>MCP-RFPT* stocks were maintained in the dark as a double homozygous line. Two types of *sog-MS2* strains were used, both CRISPR alleles containing 24MS2 stem loops in the first intron. Experiments described in Fig. 2 used a *sog-MS2* stock described in McGehee and Stathopoulos (2024) and *dl^{LEXY}; nos>MCP-mCherry-nls/TM3*; data from Figs 3 and 4 used a *sog-MS2* allele described previously (Whitney et al., 2022) and *dl^{LEXY}; nos>MCP-RFPT*. For live imaging, *dl^{LEXY}; MCP-mCherry/TM3* (or *MCP-RFPT*) females were crossed to *sog-MS2* males. For smFISH, *dl^{LEXY}/dl^{LEXY}* homozygous flies were used for embryo collections.

Live imaging and quantification to determine critical windows

Live imaging for quantification of nascent transcription spots (MCP/MS2 puncta) or DL$^{mCh\text{-}LEXY}$ levels was performed as described previously (McGehee and Stathopoulos, 2024). Briefly, embryos were collected at 18°C and then hand dechorionated in the dark, using a red film (Neewer, 10087407). Embryos were oriented and then transferred to a coverslip containing heptane glue. Embryos were covered with water to prevent desiccation. Imaging occurred on a Zeiss LMS 800 with a 25× immersible objective (LCI Plan-Neofluar 25×/0.8 Imm Korr DIC M27) at 1.7 zoom and 20-21°C. A 561 nm laser at 1% laser power with 800 V gain on a GaAsP PMT detector was used to detect the MCP-mCherry signal. A 488 nm laser at 4.5% laser power was used to perform blue-light illumination. Images consist of 30 *z*-planes per timepoint at 1 µm thickness. Images were taken every ~25 s, starting as soon as the previous *z*-stack finished. Images were captured as 16 bit, with 512×512 pixel resolution, with each pixel being 0.29 µm in length and width. In addition to the previous settings, eight *sna-MS2* movies were taken using slower settings. Images were taken every ~2 min, and each *z*-slice was 1024×1024 pixels, with each pixel being 0.15 µm long. Imaging was terminated after observing gastrulation or movement of the nuclei congruent with germ band extension when gastrulation was absent or not observable. Spots were detected as described previously (McGehee and Stathopoulos, 2024). Briefly, the image is filtered using a median filter, the background is subtracted, and the image is blurred using a Gaussian filter. Then two thresholds are applied to detect the active sites of transcription and remove noise. The embryo is segmented using a different threshold, and any spots detected outside the embryo are removed. This is performed for individual time frames, such that spots are counted instantaneously and not cumulatively. This allows for visualizing decreases in the number of active sites of transcription.

The same imaging scheme was used to image the DL$^{mCh\text{-}LEXY}$, except the 561 nm laser was used at 2% laser power. To quantify the DL$^{mCh\text{-}LEXY}$ levels, we used a similar method as described previously (McGehee and Stathopoulos, 2024). Briefly, average intensity projections were segmented using MATLAB's edge function and a Laplacian of Gaussian with a standard deviation of four for the filter. Watershedding was performed using MATLAB's watershed function to disconnect any nuclei that were connected. Objects were filtered by size to remove large (i.e. two connected nuclei) or small (i.e. non-nuclei or partial nuclei) objects. Additionally, detected objects were filtered by intensity. Specifically, images were background subtracted, and an intensity threshold was applied. Objects that overlapped in both the intensity thresholded mask and the Laplacian of Gaussian mask were kept. During light exposure, objects were not filtered by intensity because nuclei are lower intensity than the cytoplasm. During mitosis, the mask from the last time point nuclei were detectable was used until nuclei became detectable again. The embryo was detected by blurring the image, and using a normalized threshold of 0.005, followed by morphological opening and closing. The boundaries of the embryo were detected and used to fit an ellipse. From the ellipse, the midline was determined, and only nuclei within 100 pixels above or below the midline were included for analysis. The average intensity was calculated for each individual nucleus at a given time point and then was averaged together for each time point and plotted as the mean±s.d.

Live imaging to study bursting kinetics

Embryos were permitted to lay for 2 h in the dark at 25°C prior to collection for live imaging. All preparation was performed in the dark with minimal illumination through a red filter. Embryos were hand dechorionated and mounted on a hydrophobic membrane prior to immersion in oil to prevent desiccation and addition of a coverslip. Live imaging was performed with an LSM 880 with Airyscan module (Zeiss). *Z*-stacks comprised of 30 planes with a spacing of 0.5 µm, and were acquired at a time resolution of 10.21 s per stack in fast Airyscan mode with laser power measured and maintained at 14.5 µW using a ThorLabs PM100 optical power meter. All movies were performed with the following settings: constant LEXY export by a 488 nm laser and RFP excitation by a 561 nm were captured on a GaAsP-PMT array with an Airyscan detector using a 40× Plan Apo oil lens (1.3 NA) at 2.0 zoom on the lateral region of the embryo from the presumptive mesoderm to the dorsal border of the *sog* domain. Resolution was 104.7 µm×104.7 µm with bidirectional scanning. Airyscan processing was performed using 3D Zen Black v3.2 (Zeiss).

Live imaging analysis for transcriptional kinetics

Data were acquired in TZXY for each channel. A custom software was developed in Python™ (see Table S1) to detect and track MS2/MCP puncta in the absence of a nuclear marker.

Briefly, Airyscan-processed data were loaded, concatenated and maximum intensity projected for visualization purposes. To detect transcription puncta, raw data were filtered with a 3D Laplacian of Gaussian filter followed by manual thresholding based on the mean and standard deviation of the filtered image. Rare cases of optically resolvable sister chromatid separation were resolved by merging objects with a distance smaller than a user-defined threshold (generally 1-2 pixel). A volume threshold was applied to remove false detection events due to noise. Finally, spots were tracked through time using a 2D minimal distance criteria with a threshold distance to block erroneous associations. A gap of eight frames or fewer during tracking with a spot reappearing within the distance threshold was considered a continuous trace, whereas gaps of more than eight frames

Development (2025) 152, dev204706. doi:10.1242/dev.204706

were considered new detection events. Traces that were artificially short relative to the length of the nuclear cycle were eliminated.

Following tracking, background estimation was performed in 3D for each independent frame as the average intensity value of the pixels surrounding the spot. Final spot intensities were then expressed as their values divided by this estimated background to ameliorate technical error such as laser power fluctuation and *z*-dependent fluorescence intensity changes. This rescaling technique is sufficient unless photobleaching is too high. To monitor overall photobleaching, the overall behavior of the intensity on all the 4D stack excluding the transcriptional puncta was estimated, as intensity variation is driven by biological factors. All non-signal pixels per time frame were summed and used to estimate bleaching, which was measured to reach 30% at the end of 30 min (Fig. S1F). In nc13, the entire imaged region was used for analysis, and in nc14 the imaged region was divided into either ventral or lateral domains based on the presence of the mesoderm/neurogenic ectoderm border (dark control) or the position of the failing gastrulation furrow (DL exported).

Bleaching analysis

To monitor photobleaching, the overall behavior of the intensity on all the 4D stack excluding the transcriptional puncta was estimated, as intensity variation is driven by biological factors. The intensity of all non-signal pixels throughout nc14 were summed independently for each time point and movie, and fitted with an exponential decay function. For spot counting (*twi-MS2*; Fig. S3A) and $dl^{mch\text{-}LEXY}$ (Fig. S2E) movies, bleaching was analyzed for 30 min following the peak of the background signal in nc14. For *sog-MS2* bursting movies (Fig. S3B), bleaching was analyzed from the onset of nc14.

smFISH

dl^{LEXY} homozygous flies were permitted to lay for 2 h in the dark, followed by incubation of the embryos in blue light (30% power, 0.67 duty cycle) for a further 2 h in an optobox, or incubation for a further 2 h in the dark as appropriate. Embryos were fixed in 10% formaldehyde/heptane under blue light or in the dark as appropriate for 25 min with shaking before a methanol quench and stored at −20°C in methanol before use.

smFISH probes targeting *twi* conjugated to Quasar-570 (LGC Biosearch Technologies) were designed and used as previously described (Dufourt et al., 2021). smFISH probes targeting the 5′ region of the *sog* transcript were designed using Oligostan (Integrated DNA Technologies) (Tsanov et al., 2016). Probes were resuspended in Tris-EDTA buffer at equimolar concentrations. Embryos were prepared for smFISH as previously described (Pimmett et al., 2021) before mounting in ProLong Gold mounting medium (Life Technologies).

Immunofluorescence

dl^{LEXY}/dl^{LEXY} homozygous embryos were collected as described above for smFISH. Embryos were progressively rehydrated in PBS with 0.1% Tween 20 (PBT) before blocking in PBT and 0.5% bovine serum albumin, followed by incubation overnight at 4°C with mouse anti-DL (1:500; Developmental Studies Hybridoma Bank) and rabbit anti-Sna (1:800; see below). Embryos were washed four times in PBT followed by 2 h of incubation with donkey anti-mouse Alexa Fluor 488 (1:1000; Life Technologies), donkey anti-rabbit Alexa Fluor 647 (1/500, Life Technologies) and DAPI (1:1000). Embryos were washed four times in PBT before mounting in ProLong Gold mounting medium (Life Technologies).

Anti-Sna antibody was produced by Genscript as a custom rabbit antibody (polyclonal) using the full length Snail protein as the antigen (also produced by Genscript) and purified with a 6xHIS N-terminal tag, followed by antibody purification using an antigen affinity purification. The antibody was validated by showing that it lacks staining when *snail* transcript is absent (e.g. see Fig. S1F,G).

Fixed-sample imaging and analysis

For smFISH, imaging was performed on an LSM 880 with Airyscan module (Zeiss). *Z*-planes were acquired with 0.3 µm spacing spanning the entire nuclear volume, using laser scanning confocal in Airyscan super-resolution mode with a zoom of 3.0. DAPI excitation was performed with a 405 nm laser, Alexa Fluor 488 excitation with a 488 nm laser and Q580 excitation with a 561 nm laser. Detection was performed using a GaAsP-PMT array coupled to an Airyscan detector. Laser power was maintained between all channels by intensity measurement prior to imaging (ThorLabs). Airyscan processing was performed using 3D Zen Black v3.2 (Zeiss) prior to analysis. Embryos were staged based on membrane invagination.

Analysis was performed using previously published custom software (Dufourt et al., 2021). For DL and Sna nuclear level analysis (Fig. S1D,F), a post-processing tool was developed to spatially define rows of nuclei orthogonal to the dorsoventral axis by isolating the centroid of each nucleus and defining the number of bins based on the square root of the total number of nuclei in the image. Nuclei were clustered into bins based on the appropriate dorsoventral axis coordinate of the centroid. For smFISH analysis, mesoderm nuclei were defined as having twi^{+} TS signal in the nucleus.

Mathematical modeling

To ensure a stable transcriptional dynamic and to avoid any confounding factors due to bleaching during nc14, we limited the analysis window to the first 15 min after active transcription began (Fig. S6G-I). We estimate that this corresponds to the first 20-22 min after mitosis based on the post-mitotic reactivation window from previously published live-imaging studies of *sog* in nc14 (Whitney et al., 2022). For nc13, the entire nuclear cycle was retained for analysis as transcription reached and maintained a steady state (Fig. 3J).

Subsequently, the analysis was conducted in three parts. The first part involved determining the distribution of post-mitotic reactivation times. The reactivation time has two components: a deterministic component, which is the same for all nuclei, and a stochastic component, which varies among nuclei. Like in Dufourt et al. (2018), we estimated the stochastic component by setting as time origin the time when the first nucleus activates.

The second part involved determining repression onset time detection. For the determination of this time, we used a BCPD method. This method, introduced in Adams and MacKay (2007 preprint) models the statistics of the signal and identifies changepoints, i.e. moments when the signal's statistical properties change (Adams and MacKay, 2007 preprint). The BCPD method has already been tested on time-inhomogeneous live transcription in *Drosophila* embryos (Pimmett et al., 2024 preprint).

The third part uses BurstDECONV (Douaihy et al., 2023; Tantale et al., 2021) to determine the transcriptional bursting kinetic parameters for stationary segments of the signal. When the signal is repressed, the signal segment after repression onset is considered stationary. BurstDECONV first deconvolves the MS2 signal and infers the positions of the transcription initiation events. The distribution of waiting times between successive events is modeled as a multi-exponential distribution. Finally, the parameters of the multiexponential distribution are used to calculate the kinetic parameters of Markovian transcriptional bursting models assumed to function at stationarity. This method has been tested on live transcription data from *Drosophila* embryos and human cells, as well as on synthetic datasets (Douaihy et al., 2023; Pimmett et al., 2021; Tantale et al., 2021), and has rigorous probabilistic and algebraic foundations (Radulescu et al., 2023).

For the extraction of kinetic parameters, it was imperative to ensure that we were in a steady-state regime. To study the homogeneity of the signal, we estimated the mean waiting time between successive polymerase initiation denoted $\langle\tau\rangle$ across a narrow moving window. This value, for each window, is related to the product of p_{ON}, the probability that the promoter is ON, and k_{INI}, the initiation rate in the ON state. Therefore, if $\langle\tau\rangle$ is constant across different time windows, then the product of p_{ON} (the probability that transcription is active) and k_{INI} (the transcription initiation rate in the active state; here, it is assumed that initiation does not occur in the inactive states) is constant, suggesting that the kinetic parameters are constant (see Pimmett et al., 2024 preprint for more details). The width of the moving window used here is eight frames, or 82 s. We used this moving window to show that the kinetic parameters are constant on a maximal duration of 15 min after the first activation of the first nuclei in each movie. Finally, using time series of this maximal duration, we were able to apply our existing pipeline to extract kinetic parameters and perform transcriptional bursting model selection (Douaihy et al., 2023). The hyperparameters used for the BurstDECONV pipeline are as follows: a Pol II speed of 25 bp/s (equivalent to a dwell time of 414 s); a time resolution of 10.21; and distances between the transcription start site and the start of MS2 loops, the size of the MS2 loops, and the distance between the end

of the MS2 loops and the 3′ splice site of 2553 bp, 1267 bp and 9081 bp, respectively. Given the insertion of the MS2 sequence into the intron, persistence of the MS2 signal at the TS will be reduced if the intron is removed via splicing, thus impacting the signal deconvolution (Ferraro et al., 2016). We ensured that *sog* splicing was not recursive at this stage by consulting NET-seq data from *Drosophila* embryos (Prudêncio et al., 2022). Instead, *sog* splicing likely occurs at intron-exon junctions and co-transcriptionally as supported by FISH data (Bothma et al., 2011). We considered both two-state (random telegraph) and three-state Markovian transcriptional bursting models as shown in Fig. 3K,L and Fig. S6J-L.

Acknowledgements
We are grateful to Eileen Furlong and Alessandro Dulja (EMBL, Heidelberg) for help with setting up the optobox; Sarah Bray, Hernan Garcia and Chris Rushlow for providing fly stocks; Mike Levine for providing plasmid DNA; and Louise Maillard and Leslie Dunipace for comments on the manuscript. We also thank Pedro Prudêncio (Carmo Fonseca laboratory) and Amal Makrini (IGMM, CNRS) for the analysis of published NET-seq data. We acknowledge imaging and technical support from the Montpellier Ressources Imagerie facility (France-BioImaging), the Biocampus *Drosophila* facility of Montpellier and the Caltech Beckman Institute Imaging Facility.

Competing interests
The authors declare no competing or financial interests.

Author contributions
Conceptualization: V.L.P., J.M., A.S., M.L.; Data curation: V.L.P., J.M., A.T.; Formal analysis: V.L.P., J.M., A.T., M.D., O.R.; Funding acquisition: A.S., M.L.; Investigation: V.L.P., J.M., M.D.; Methodology: M.L., A.S., O.R., V.L.P., M.D., J.M., A.T.; Project administration: A.S., M.L.; Resources: A.S., M.L.; Software: J.M., A.T., O.R.; Supervision: O.R., A.S., M.L.; Visualization: V.L.P., J.M.; Writing – original draft: V.L.P., J.M., A.S., M.L.; Writing – review & editing: V.L.P., J.M., A.T., M.D., A.S., M.L., O.R.

Funding
This study was supported by funding from the National Institutes of Health (R35GM118146 to A.S.), as well as the European Research Council (ERC) SyncDev and Agence Nationale de la Recherche (ANR) HubDyn (to M.L.). M.D. is supported by the Centre National de la Recherche Scientifique (CNRS) and University of Chicago joint PhD program. V.L.P. was initially supported by ERC SyncDev and then ANR HubDyn. M.L., O.R., and A.T. are sponsored by CNRS. Open Access funding provided by the California Institute of Technology. Deposited in PMC for immediate release.

Data and resource availability
Codes for quantitative analyses are available at GitHub (see Table S1 for links).

References
Adams, R. P. and MacKay, D. J. C. (2007). Bayesian online changepoint detection. *arXiv* 0710.3742. doi:10.48550/arXiv.0710.3742

Bellec, M., Radulescu, O. and Lagha, M. (2018). Remembering the past: Mitotic bookmarking in a developing embryo. *Curr. Opin. Syst. Biol.* **11**, 41-49. doi:10.1016/j.coisb.2018.08.003

Bellec, M., Dufourt, J., Hunt, G., Lenden-Hasse, H., Trullo, A., Zine El Aabidine, A., Lamarque, M., Gaskill, M. M., Faure-Gautron, H., Mannervik, M. et al. (2022). The control of transcriptional memory by stable mitotic bookmarking. *Nat. Commun.* **13**, 1176. doi:10.1038/s41467-022-28855-y

Berrocal, A., Lammer, N. C., Garcia, H. G. and Eisen, M. B. (2024). Unified bursting strategies in ectopic and endogenous even-skipped expression patterns. *eLife* **12**, RP88671. doi:10.7554/eLife.88671.3

Bothma, J. P., Magliocco, J. and Levine, M. (2011). The snail repressor inhibits release, not elongation, of paused Pol II in the Drosophila embryo. *Curr. Biol.* **21**, 1571-1577. doi:10.1016/j.cub.2011.08.019

Bothma, J. P., Garcia, H. G., Ng, S., Perry, M. W., Gregor, T. and Levine, M. (2015). Enhancer additivity and non-additivity are determined by enhancer strength in the Drosophila embryo. *eLife* **4**, e07956. Preprint at. doi:10.7554/elife.07956

Briscoe, J. and Small, S. (2015). Morphogen rules: design principles of gradient-mediated embryo patterning. *Development* **142**, 3996-4009. doi:10.1242/dev.129452

Chen, P.-T., Zoller, B., Levo, M. and Gregor, T. (2023). Gene activity as the predictive indicator for transcriptional bursting dynamics. *arXiv*. doi:10.48550/arXiv.2304.08770

Chopra, V. S. and Levine, M. (2009). Combinatorial patterning mechanisms in the Drosophila embryo. *Brief. Funct. Genomic. Proteomic.* **8**, 243-249. doi:10.1093/bfgp/elp026

Chopra, V. S., Kong, N. and Levine, M. (2012). Transcriptional repression via antilooping in the Drosophila embryo. *Proc. Natl. Acad. Sci. USA* **109**, 9460-9464. doi:10.1073/pnas.1102625108

Davidson, E. H. (2010). Emerging properties of animal gene regulatory networks. *Nature* **468**, 911-920. doi:10.1038/nature09645

DeLotto, R., DeLotto, Y., Steward, R. and Lippincott-Schwartz, J. (2007). Nucleocytoplasmic shuttling mediates the dynamic maintenance of nuclear Dorsal levels during Drosophila embryogenesis. *Development* **134**, 4233-4241. doi:10.1242/dev.010934

Douaihy, M., Topno, R., Lagha, M., Bertrand, E. and Radulescu, O. (2023). BurstDECONV: a signal deconvolution method to uncover mechanisms of transcriptional bursting in live cells. *Nucleic Acids Res.* **51**, e88. doi:10.1093/nar/gkad629

Dufourt, J., Trullo, A., Hunter, J., Fernandez, C., Lazaro, J., Dejean, M., Morales, L., Nait-Amer, S., Schulz, K. N., Harrison, M. M. et al. (2018). Temporal control of gene expression by the pioneer factor Zelda through transient interactions in hubs. *Nat. Commun.* **9**, 5194. doi:10.1038/s41467-018-07613-z

Dufourt, J., Bellec, M., Trullo, A., Dejean, M., De Rossi, S., Favard, C. and Lagha, M. (2021). Imaging translation dynamics in live embryos reveals spatial heterogeneities. *Science* **372**, 840-844. doi:10.1126/science.abc3483

Dunipace, L., Ákos, Z. and Stathopoulos, A. (2019). Coacting enhancers can have complementary functions within gene regulatory networks and promote canalization. *PLoS Genet.* **15**, e1008525. doi:10.1371/journal.pgen.1008525

Economou, A. D. and Hill, C. S. (2020). Temporal dynamics in the formation and interpretation of Nodal and BMP morphogen gradients. *Curr. Top. Dev. Biol.* **137**, 363-389. doi:10.1016/bs.ctdb.2019.10.012

Esposito, E., Lim, B., Guessous, G., Falahati, H. and Levine, M. (2016). Mitosis-associated repression in development. *Genes Dev.* **30**, 1503-1508. doi:10.1101/gad.281188.116

Falo-Sanjuan, J. and Bray, S. (2022). Notch-dependent and -independent transcription are modulated by tissue movements at gastrulation. *eLife* **11**, e73656. doi:10.7554/eLife.73656

Fernandez, C. and Lagha, M. (2019). Lighting up gene activation in living Drosophila embryos. *Methods Mol. Biol.* **2038**, 63-74. doi:10.1007/978-1-4939-9674-2_5

Ferraro, T., Lucas, T., Clémot, M., De Las Heras Chanes, J., Desponds, J., Coppey, M., Walczak, A. M. and Dostatni, N. (2016). New methods to image transcription in living fly embryos: the insights so far, and the prospects. *Wiley Interdiscip. Rev. Dev. Biol.* **5**, 296-310. doi:10.1002/wdev.221

Forbes Beadle, L., Zhou, H., Rattray, M. and Ashe, H. L. (2023). Modulation of transcription burst amplitude underpins dosage compensation in the Drosophila embryo. *Cell Rep.* **42**, 112382. doi:10.1016/j.celrep.2023.112382

Garcia, H. G., Tikhonov, M., Lin, A. and Gregor, T. (2013). Quantitative imaging of transcription in living Drosophila embryos links polymerase activity to patterning. *Curr. Biol.* **23**, 2140-2145. doi:10.1016/j.cub.2013.08.054

Gratz, S. J., Ukken, F. P., Rubinstein, C. D., Thiede, G., Donohue, L. K., Cummings, A. M. and O'Connor-Giles, K. M. (2014). Highly specific and efficient CRISPR/Cas9-catalyzed homology-directed repair in Drosophila. *Genetics* **196**, 961-971. doi:10.1534/genetics.113.160713

Hoppe, C., Bowles, J. R., Minchington, T. G., Sutcliffe, C., Upadhyai, P., Rattray, M. and Ashe, H. L. (2020). Modulation of the promoter activation rate dictates the transcriptional response to graded BMP signaling levels in the Drosophila embryo. *Dev. Cell* **54**, 727-741.e7. doi:10.1016/j.devcel.2020.07.007

Huang, A., Amourda, C., Zhang, S., Tolwinski, N. S. and Saunders, T. E. (2017). Decoding temporal interpretation of the morphogen Bicoid in the early embryo. *eLife* **6**, e26258. doi:10.7554/eLife.26258

Irizarry, J., McGehee, J., Kim, G., Stein, D. and Stathopoulos, A. (2020). Twist-dependent ratchet functioning downstream from Dorsal revealed using a light-inducible degron. *Genes Dev.* **34**, 965-972. doi:10.1101/gad.338194.120

Javier DeHaro-Arbona, F., Roussos, C., Baloul, S., Townson, J., Gómez Lamarca, M. J. and Bray, S. (2024). Dynamic modes of Notch transcription hubs conferring memory and stochastic activation revealed by live imaging the co-activator Mastermind. *eLife* **12**, RP92083. doi:10.7554/eLife.92083.3

Kanodia, J. S., Rikhy, R., Kim, Y., Lund, V. K., Delotto, R., Lippincott-Schwartz, J. and Shvartsman, S. Y. (2009). Dynamics of the Dorsal morphogen gradient. *Proc. Natl. Acad. Sci. USA* **106**, 21707-21712. doi:10.1073/pnas.0912395106

Kögler, A. C., Kherdjemil, Y., Bender, K., Rabinowitz, A., Marco-Ferreres, R. and Furlong, E. E. M. (2021). Extremely rapid and reversible optogenetic perturbation of nuclear proteins in living embryos. *Dev. Cell* **56**, 2348-2363.e8. doi:10.1016/j.devcel.2021.07.011

Kosman, D., Ip, Y. T., Levine, M. and Arora, K. (1991). Establishment of the mesoderm-neuroectoderm boundary in the Drosophila embryo. *Science* **254**, 118-122. doi:10.1126/science.1925551

Kutejova, E., Briscoe, J. and Kicheva, A. (2009). Temporal dynamics of patterning by morphogen gradients. *Curr. Opin. Genet. Dev.* **19**, 315-322. doi:10.1016/j.gde.2009.05.004

Lammers, N. C., Kim, Y. J., Zhao, J. and Garcia, H. G. (2020). A matter of time: using dynamics and theory to uncover mechanisms of transcriptional bursting. *Curr. Opin. Cell Biol.* **67**, 147-157. doi:10.1016/j.ceb.2020.08.001

Leptin, M. (1991). twist and snail as positive and negative regulators during Drosophila mesoderm development. *Genes Dev.* **5**, 1568-1576. doi:10.1101/gad.5.9.1568

Leptin, M. and Grunewald, B. (1990). Cell shape changes during gastrulation in Drosophila. *Development* **110**, 73-84. doi:10.1242/dev.110.1.73

Lucas, T., Ferraro, T., Roelens, B., De Las Heras Chanes, J., Walczak, A. M., Coppey, M. and Dostatni, N. (2013). Live imaging of bicoid-dependent transcription in Drosophila embryos. *Curr. Biol.* **23**, 2135-2139. doi:10.1016/j.cub.2013.08.053

Manu, Surkova, S., Spirov, A. V., Gursky, V. V., Janssens, H., Kim, A.-R., Radulescu, O., Vanario-Alonso, C. E., Sharp, D. H., Samsonova, M. et al. (2009). Canalization of gene expression in the Drosophila blastoderm by gap gene cross regulation. *PLoS Biol.* **7**, e1000049. doi:10.1371/journal.pbio.1000049

McFann, S., Dutta, S., Toettcher, J. E. and Shvartsman, S. Y. (2021). Temporal integration of inductive cues on the way to gastrulation. *Proc. Natl. Acad. Sci. USA* **118**, e2102691118. doi:10.1073/pnas.2102691118

McGehee, J. and Stathopoulos, A. (2024). Target gene responses differ when transcription factor levels are acutely decreased by nuclear export versus degradation. *Development* **151**, e1009040. (2024: epub 14 Oct). doi:10.1242/dev.202775

McHale, P., Mizutani, C. M., Kosman, D., MacKay, D. L., Belu, M., Hermann, A., McGinnis, W., Bier, E. and Hwa, T. (2011). Gene length may contribute to graded transcriptional responses in the Drosophila embryo. *Dev. Biol.* **360**, 230-240. doi:10.1016/j.ydbio.2011.08.016

Meeussen, J. V. W. and Lenstra, T. L. (2024). Time will tell: comparing timescales to gain insight into transcriptional bursting. *Trends Genet.* **40**, 160-174. doi:10.1016/j.tig.2023.11.003

Niopek, D., Wehler, P., Roensch, J., Eils, R. and Di Ventura, B. (2016). Optogenetic control of nuclear protein export. *Nat. Commun.* **7**, 10624. doi:10.1038/ncomms10624

Perry, M. W., Boettiger, A. N., Bothma, J. P. and Levine, M. (2010). Shadow enhancers foster robustness of Drosophila gastrulation. *Curr. Biol.* **20**, 1562-1567. doi:10.1016/j.cub.2010.07.043

Pimmett, V. L., Dejean, M., Fernandez, C., Trullo, A., Bertrand, E., Radulescu, O. and Lagha, M. (2021). Quantitative imaging of transcription in living Drosophila embryos reveals the impact of core promoter motifs on promoter state dynamics. *Nat. Commun.* **12**, 4504. doi:10.1038/s41467-021-24461-6

Pimmett, V., Douaihy, M., Maillard, L., Trullo, A., Garcia-Idieder, P., Costes, M., Dufourt, J., Lenden-Hasse, H., Radulescu, O. and Lagha, M. (2024). Coordinated active repression operates via transcription factor cooperativity and multiple inactive promoter states in a developing organism. *bioRxiv* doi:10.1101/2024.02.05.577724

Prudêncio, P., Savisaar, R., Rebelo, K., Martinho, R. G. and Carmo-Fonseca, M. (2022). Transcription and splicing dynamics during early development. *RNA* **28**, 139-161. doi:10.1261/rna.078933.121

Radulescu, O., Grigoriev, D., Seiss, M., Douaihy, M., Lagha, M. and Bertrand, E. (2023). Identifying Markov chain models from time-to-event data: an algebraic approach. *Bull. Math. Biol.* **87**, 11. doi:10.1007/s11538-024-01385-y

Reeves, G. T. and Stathopoulos, A. (2009). Graded dorsal and differential gene regulation in the Drosophila embryo. *Cold Spring Harb. Perspect. Biol.* **1**, a000836. doi:10.1101/cshperspect.a000836

Reeves, G. T., Trisnadi, N., Truong, T. V., Nahmad, M., Katz, S. and Stathopoulos, A. (2012). Dorsal-ventral gene expression in the Drosophila embryo reflects the dynamics and precision of the dorsal nuclear gradient. *Dev. Cell* **22**, 544-557. doi:10.1016/j.devcel.2011.12.007

Rembold, M., Ciglar, L., Yáñez-Cuna, J. O., Zinzen, R. P., Girardot, C., Jain, A., Welte, M. A., Stark, A., Leptin, M. and Furlong, E. E. M. (2014). A conserved role for Snail as a potentiator of active transcription. *Genes Dev.* **28**, 167-181. doi:10.1101/gad.230953.113

Schloop, A. E., Bandodkar, P. U. and Reeves, G. T. (2020). Formation, interpretation, and regulation of the Drosophila Dorsal/NF-κB gradient. *Curr. Top. Dev. Biol.* **137**, 143-191. doi:10.1016/bs.ctdb.2019.11.007

Tantale, K., Garcia-Oliver, E., Robert, M.-C., L'Hostis, A., Yang, Y., Tsanov, N., Topno, R., Gostan, T., Kozulic-Pirher, A., Basu-Shrivastava, M. et al. (2021). Stochastic pausing at latent HIV-1 promoters generates transcriptional bursting. *Nat. Commun.* **12**, 4503. doi:10.1038/s41467-021-24462-5

Tsanov, N., Samacoits, A., Chouaib, R., Traboulsi, A.-M., Gostan, T., Weber, C., Zimmer, C., Zibara, K., Walter, T., Peter, M. et al. (2016). smiFISH and FISH-quant - a flexible single RNA detection approach with super-resolution capability. *Nucleic Acids Res.* **44**, e165. doi:10.1093/nar/gkw784

Wan, Y., Anastasakis, D. G., Rodriguez, J., Palangat, M., Gudla, P., Zaki, G., Tandon, M., Pegoraro, G., Chow, C. C., Hafner, M. et al. (2021). Dynamic imaging of nascent RNA reveals general principles of transcription dynamics and stochastic splice site selection. *Cell* **184**, 2878-2895.e20. doi:10.1016/j.cell.2021.04.012

Whitney, P. H., Shrestha, B., Xiong, J., Zhang, T. and Rushlow, C. A. (2022). Shadow enhancers modulate distinct transcriptional parameters that differentially effect downstream patterning events. *Development* **149**, dev200940. doi:10.1242/dev.200940

Yamada, S., Whitney, P. H., Huang, S.-K., Eck, E. C., Garcia, H. G. and Rushlow, C. A. (2019). The *Drosophila* pioneer factor Zelda modulates the nuclear microenvironment of a dorsal target enhancer to potentiate transcriptional output. *Curr. Biol.* **29**, 1387-1393.e5. doi:10.1016/j.cub.2019.03.019